

# Microscopic cluster model for the description of new experimental results on the $^{13}\text{C}(^{18}\text{O}, ^{16}\text{O})^{15}\text{C}$ two-neutron transfer at 84 MeV incident energy

D. Carbone,<sup>1,\*</sup> J. L. Ferreira,<sup>2</sup> F. Cappuzzello,<sup>1,3</sup> J. Lubian,<sup>2</sup> C. Agodi,<sup>1</sup> M. Cavallaro,<sup>1</sup> A. Foti,<sup>3,4</sup>  
A. Gargano,<sup>5</sup> S. M. Lenzi,<sup>6</sup> R. Linares,<sup>2</sup> and G. Santagati<sup>1</sup>

<sup>1</sup>*INFN Laboratori Nazionali del Sud, Catania, Italy*

<sup>2</sup>*Instituto de Fisica, Universidade Federal Fluminense, Niteroi, Rio de Janeiro, Brazil*

<sup>3</sup>*Dipartimento di Fisica e Astronomia, Università degli Studi di Catania, Italy*

<sup>4</sup>*INFN Sezione di Catania, Catania, Italy*

<sup>5</sup>*INFN Sezione di Napoli, Napoli, Italy*

<sup>6</sup>*INFN Sezione di Padova, Padova, Italy*

(Received 17 October 2016; published 9 March 2017)

The  $^{13}\text{C}(^{18}\text{O}, ^{16}\text{O})^{15}\text{C}$  reaction is studied at 84 MeV incident energy. Excitation energy spectra and absolute cross-section angular distributions for the strongest transitions are measured with good energy and angular resolutions. Strong selectivity for two-neutron configurations in the states of the residual nucleus is found. The measured cross-section angular distributions are analyzed by exact finite-range coupled reaction channel calculations. The two-particle wave functions are extracted using the extreme cluster and the independent coordinate scheme with shell-model derived coupling strengths. A new approach also is introduced, the microscopic cluster, in which the spectroscopic amplitudes in the center-of-mass reference frame are derived from shell-model calculations using the Moshinsky transformation brackets. This new model is able to describe well the experimental cross section and to highlight cluster configurations in the involved wave functions.

DOI: [10.1103/PhysRevC.95.034603](https://doi.org/10.1103/PhysRevC.95.034603)

## I. INTRODUCTION

The study of the atomic nucleus is a very difficult task since it is a complex many-body system. Focusing on some precise degrees of freedom can help to understand some specific features of it, such as pairing correlations, single-particle states, collective states, and more [1]. In this context, direct two-nucleon transfer reactions play an important role, and indeed they were extensively explored [2–9] to study pairing correlations. Among these, heavy-ion direct transfer reactions at energies close to the Coulomb barrier are useful tools for obtaining precise spectroscopic information. Over the past few years, a systematic study on heavy-ion-induced one- and two-neutron transfer reactions on different target nuclei was pursued at the Istituto Nazionale di Fisica Nucleare-Laboratori Nazionali del Sud (INFN-LNS) (Italy) by the  $(^{18}\text{O}, ^{17}\text{O})$  and  $(^{18}\text{O}, ^{16}\text{O})$  reactions at incident energies ranging from 84 to 270 MeV. Many nuclear systems were explored using  $^9\text{Be}$ ,  $^{11}\text{B}$ ,  $^{12}\text{C}$ ,  $^{13}\text{C}$ ,  $^{16}\text{O}$ ,  $^{28}\text{Si}$ , and  $^{64}\text{Ni}$  targets and the MAGNEX spectrometer [10–12] to detect the ejectiles. Thanks to the spectrometer's high resolution and large acceptance, high quality inclusive spectra were obtained, even in a largely unexplored region above the two-neutron separation energy in the residual nucleus [13–17]. New phenomena were unveiled, such as the dominance of the direct one-step transfer of the two neutrons [18] and the presence of broad resonances at high excitation energy in the  $^{14}\text{C}$  and  $^{15}\text{C}$  spectra. The latter recently were associated with an experimental indication of the giant pairing vibration [19,20]. A thorough analysis of the broad structures populated in the  $^{13}\text{C}(^{18}\text{O}, ^{16}\text{O})^{15}\text{C}$  reaction

at high excitation energy above the two-neutron emission threshold was presented in Ref. [21], and the neutron decay of these structures was investigated in Ref. [22] thanks to the use of the EDEN array coupled to the spectrometer [23,24]. Moreover, it was demonstrated that the  $(^{18}\text{O}, ^{16}\text{O})$  two-neutron transfer reaction can be used for quantitative spectroscopic studies of pair configurations in nuclear states [25,26]. The  $^{12}\text{C}(^{18}\text{O}, ^{16}\text{O})^{14}\text{C}$  is found to selectively populate two-neutron configurations in the states of the residual  $^{14}\text{C}$  nucleus, similar to the corresponding  $(t, p)$  reaction [2,27].

From a theoretical point of view, a complete treatment of the transfer process should contain a description of: (i) the one-step channel (transition between the partitions  $\alpha \rightarrow \beta$ ) with the inclusion of all the possible inelastic excitations of the target, projectile, ejectile, or residual nucleus; (ii) the sequential channel with the inclusion of intermediate partitions  $\gamma$ , and (iii) the nonorthogonal term deriving from the limited model space used in actual calculations in both the (i) and the (ii) approaches. However, such a complete model is still not available in the state-of-the-art theories.

A possible way to describe the two-neutron transfer reactions is the second-order distorted-wave Born approximation (DWBA) approach, recently applied in Refs. [7,9] to calculate the absolute differential cross sections for the  $(p, t)$  reactions on tin isotopes. Nevertheless, these calculations do not take into account the inelastic excitations of the involved nuclei, which are relevant routes when considering heavy-ion-induced reactions [28–30]. In such cases, it is necessary to explicitly include them by using the coupled-channel approach. With the lack of a complete two-step coupled reaction channel (CRC) theory, the one-step and two-step calculations can be performed separately and their amplitudes summed by considering the relative phase as an additional parameter.

\*Corresponding author: [carboned@lns.infn.it](mailto:carboned@lns.infn.it)

This procedure is a better approximation than excluding the inelastic excitations as in pure DWBA approaches in the cases where one of the two amplitudes is much larger than the other, which is a typical situation for the ( $^{18}\text{O}, ^{16}\text{O}$ ) reaction at energies close to the Coulomb barrier [25,26].

In Ref. [25] the experimental absolute cross sections of the one- and two-neutron transfer reactions induced by an  $^{18}\text{O}$  beam on a  $^{12}\text{C}$  target were reproduced for the first time without the need for any scaling factor by means of exact finite-range CRC calculations. Two approaches were used: the extreme cluster model and the independent coordinate scheme. The description of these approaches can be found in Refs. [31,32], respectively. The relevance of the cluster configurations was revealed in the ground-state (g.s.) wave function of the  $^{14}\text{C}$  nucleus, which was described accurately within the extreme cluster approach. However, the strong approximation adopted in the extreme cluster approach makes it useful only in a few cases, e.g., it does not describe well the higher excitation energy states of  $^{14}\text{C}$  [25]. On the contrary, the independent coordinate scheme gives an accurate description of the cross-section angular distributions provided that an appropriate model space is available, but it does not highlight possible cluster configurations in the wave functions.

In this paper, we analyze the absolute cross-section angular distributions of the transitions below the two-neutron separation energy populated by the  $^{13}\text{C}(^{18}\text{O}, ^{16}\text{O})^{15}\text{C}$  two-neutron transfer reaction at 84 MeV incident energy. These are treated in the same framework of our previous work [25] to study the effect of the extra neutron in  $^{13}\text{C}$  with respect to  $^{12}\text{C}$  in the reaction dynamics. Moreover, a new approach consisting of a fully microscopic cluster calculation is introduced, performed by using the two-neutron spectroscopic amplitudes calculated in the shell-model framework. This new approach can be used more extensively with respect to the extreme cluster to evaluate the presence of cluster components in the involved wave functions.

## II. THE EXPERIMENT

The experiment was performed at the INFN-LNS laboratory in Catania. The beam of  $^{18}\text{O}^{6+}$ , accelerated at 84 MeV incident energy by the Tandem Van de Graaff accelerator, impinged on a  $50 \pm 3 \mu\text{g}/\text{cm}^2$  self-supporting 99% enriched  $^{13}\text{C}$  target, produced at the LNS chemical laboratory. Supplementary runs with a  $59 \pm 3 \mu\text{g}/\text{cm}^2$  self-supporting  $^{12}\text{C}$  target were recorded for estimating the background in the  $^{15}\text{C}$  energy spectrum coming from the  $^{12}\text{C}$  impurities in the  $^{13}\text{C}$  target. The beam-integrated charge was measured by a Faraday cup mounted 15 cm downstream of the target. The ejectiles of  $^{16}\text{O}$  were momentum analyzed by the MAGNEX spectrometer working in the full acceptance mode (solid angle of  $\Omega \sim 50$  msr and momentum range of  $\Delta p/p \sim 24\%$ ) [10]. Three angular settings were explored with the spectrometer optical axis centered at  $\theta_{\text{opt}} = 6^\circ, 12^\circ, \text{ and } 18^\circ$ . Due to the large angular acceptance of the MAGNEX, these angular settings correspond to a total covered angular range of  $3^\circ < \theta_{\text{lab}} < 24.3^\circ$  in the laboratory reference frame with an overlap of  $\sim 6^\circ$  between two consecutive runs. The particle identification and the data reduction technique are the same as described in detail

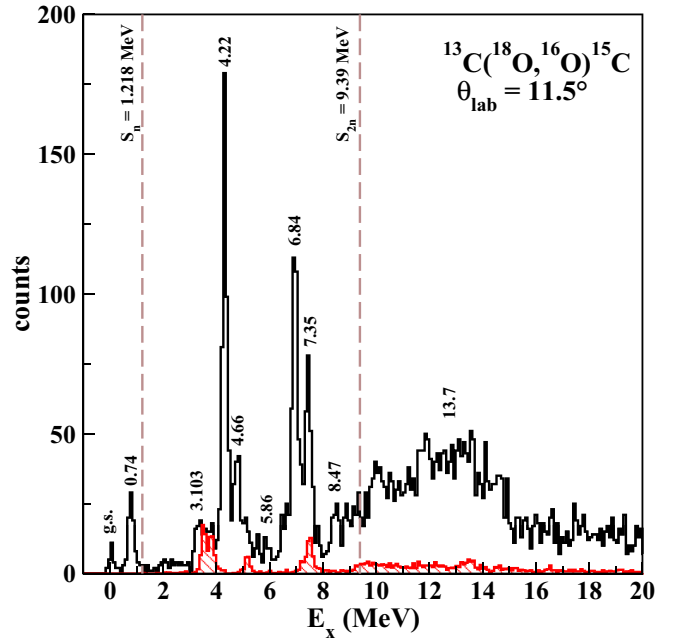


FIG. 1. Excitation energy spectrum of the  $^{13}\text{C}(^{18}\text{O}, ^{16}\text{O})^{15}\text{C}$  reaction at 84 MeV incident energy and  $11^\circ < \theta_{\text{lab}} < 12^\circ$ . The red-hatched area corresponds to the background that comes from  $^{12}\text{C}$  impurities in the target. Lines corresponding to the one- ( $S_n$ ) and two-neutron ( $S_{2n}$ ) separation energies also are indicated.

in Refs. [20,33]. The latter is based on the fully differential algebraic method implemented in the MAGNEX [34,35] and requires the horizontal and vertical positions and angles at the focal plane as inputs, which are measured by the focal plane detector [36,37].

An example of the obtained energy spectra for the  $^{15}\text{C}$  nucleus is shown in Fig. 1 in which  $E_x = Q - Q_0$ , where  $Q_0$  is the ground-state-to-ground-state reaction  $Q$  value. An overall energy resolution of  $\sim 160$  keV full width at half maximum is obtained, mainly determined by the straggling introduced by the target. The  $^{14}\text{C}$  background spectrum coming from the  $^{12}\text{C}$  impurities in the  $^{13}\text{C}$  target is superimposed after normalization on the  $^{15}\text{C}$  one in Fig. 1. Examples of the obtained absolute cross-section angular distributions for the strongest transitions are shown in Figs. 2–4. The angular resolution is  $\sim 0.3^\circ$ , the systematic error in the cross section is  $\sim 10\%$ , coming from uncertainties in the target thickness and beam integration by the Faraday cup, and it is not included in the error bars. These correspond to other sources of uncertainty, such as the solid angle determination, the statistical error, and the background subtraction.

## III. SPECTRUM DESCRIPTION

In the spectrum shown in Fig. 1, several bound and resonant states of the  $^{15}\text{C}$  nucleus are recognized. These are the same strongly populated in the ( $t, p$ ) reactions on  $^{13}\text{C}$  [38]. In particular, below the one-neutron separation energy ( $S_n = 1.218$  MeV) the only two  $^{15}\text{C}$  bound states are identified, i.e., the ground ( $J^\pi = 1/2^+$ ) and the  $5/2^+$  state at  $E_x = 0.74$  MeV. These states are characterized by dominant single-particle

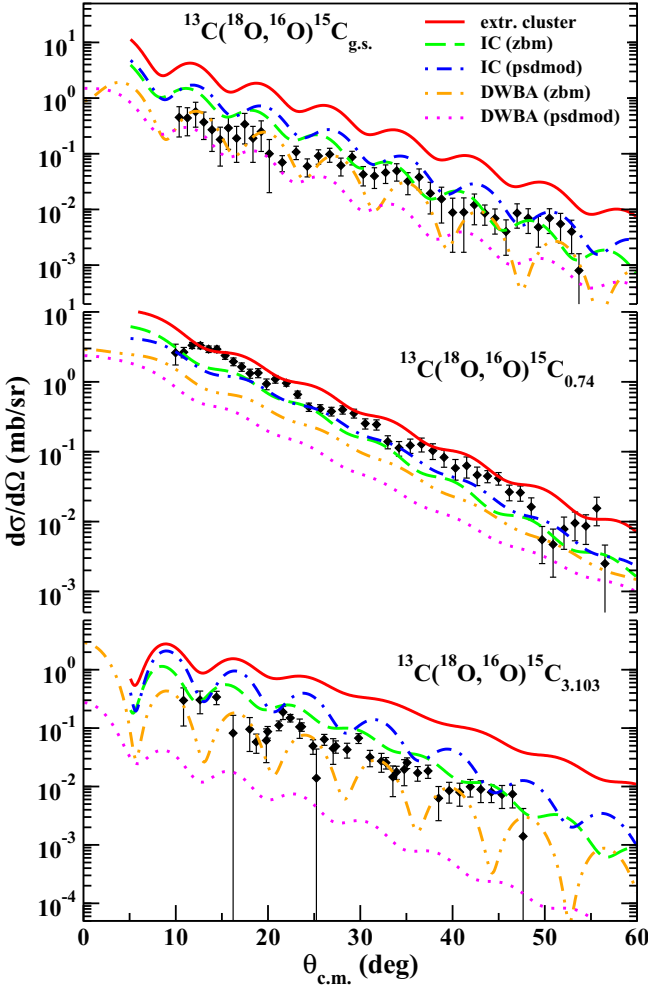


FIG. 2. Experimental cross-section angular distributions for the transitions to the ground state and states at 0.74 and 3.103 MeV in  $^{15}\text{C}$ . Theoretical calculations (see the text): extreme cluster calculations (red lines), independent coordinate calculations using the ZBM (green dashed lines) and  $ps$ - $d$ -mod (blue dashed-dotted lines) interactions, and two-step sequential DWBA calculations using the ZBM (orange dashed-double-dotted lines) and  $ps$ - $d$ -mod (magenta dotted lines) interactions.

configurations, i.e.,  $|^{15}\text{C}_{\text{g.s.}}(1/2^+)\rangle = |^{14}\text{C}_{\text{g.s.}}(0^+) \otimes (2s_{1/2})_v\rangle$  and  $|^{15}\text{C}_{0.74}(5/2^+)\rangle = |^{14}\text{C}_{\text{g.s.}}(0^+) \otimes (1d_{5/2})_v\rangle$ , both with spectroscopic factors close to 1 [39].

In the region between  $S_n$  and the two-neutron separation energy ( $S_{2n} = 9.39$  MeV), narrow resonances at  $E_x = 3.103$  ( $1/2^-$ ), 4.22 ( $5/2^-$ ), 4.66 ( $3/2^-$ ), 6.84 ( $9/2^-$ ,  $7/2^-$ ), and 7.35 ( $9/2^-$ ,  $7/2^-$ ) MeV are populated. All of these states are indicated to consist mainly of  $2p$ - $1h$  configurations (with respect to the  $^{14}\text{C}_{\text{g.s.}}$  vacuum state) i.e., a  $^{13}\text{C}+2n$  in the work by Truong and Fortune [38] (actually the authors label these states  $2p$ - $3h$  since their vacuum state is  $^{16}\text{O}_{\text{g.s.}}$ ). The doublet at 6.84 and 7.35 MeV has tentative spin assignment  $9/2^-$ ,  $7/2^-$  from Ref. [38], but recently assignments of  $9/2^-$  to the state at 6.84 MeV and  $7/2^-$  to that at 7.35 MeV were suggested by Bohlen *et al.* [40]. Resonances with a single-particle configuration of a  $^{14}\text{C}_{\text{g.s.}}+1n$ , such as those

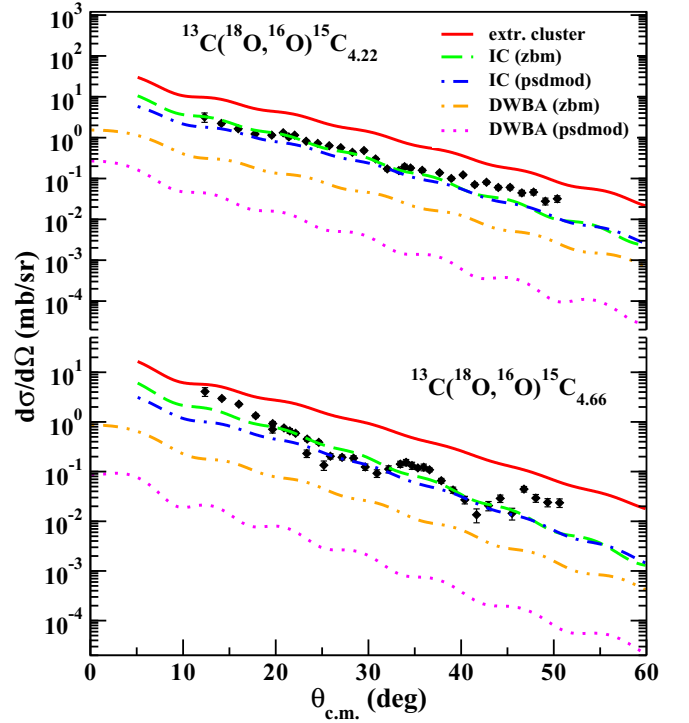


FIG. 3. Experimental cross-section angular distributions for the transitions to the 4.22 and 4.66 MeV states in  $^{15}\text{C}$ . Theoretical calculations (see the text): extreme cluster calculations (red lines), independent coordinate calculations using the ZBM (green dashed lines) and  $ps$ - $d$ -mod (blue dashed-dotted lines) interactions, and two-step sequential DWBA calculations using the ZBM (orange dashed-double-dotted lines) and  $ps$ - $d$ -mod (magenta dotted lines) interactions.

at  $E_x = 4.78, 5.86, 6.36, 6.42,$  and  $7.10$  MeV [41,42], are very weakly populated in the present reaction. Also the Fano resonance at  $E_x = 8.47$  MeV [43,44] is suppressed.

The region above the two-neutron separation energy was analyzed in previous works. A structure connected to the excitation of  $^{13}\text{C}+n+n$  configurations where the two neutrons are mainly transferred to  $d_{5/2}$  and  $d_{3/2}$  orbitals was discussed in Ref. [21], and the resonance at  $E_x = 13.7 \pm 0.1$  MeV recently was associated with the excitation of the giant pairing vibration [19,20].

#### IV. THEORETICAL ANALYSIS

Exact finite-range CRC and two-step DWBA calculations for two-neutron transfer reactions were performed to describe the cross section using the FRESKO code [45]. Nonorthogonality corrections and full complex remnant terms were used in the coupling scheme. In these calculations the São Paulo double-folding potential [46] was used as the optical potential for the real and the imaginary parts. In the entrance partition, a strength coefficient of 0.6 was used in the imaginary part to account for dissipative processes and for the missing couplings to continuum states, which were not explicitly considered [47]. In the outgoing partitions, the imaginary part was scaled by a larger factor (0.78) because no couplings were introduced.

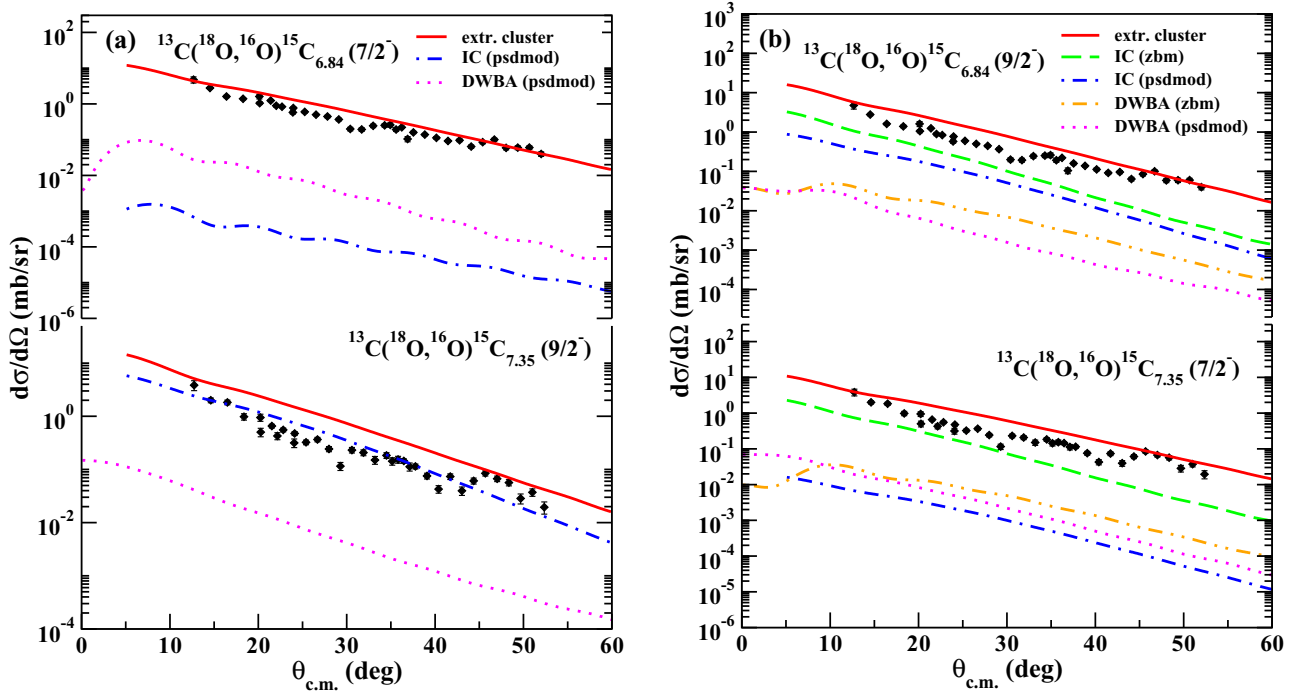


FIG. 4. Experimental cross-section angular distributions for the transitions to the 6.84 and 7.35 MeV states in  $^{15}\text{C}$ . Theoretical calculations (see the text): extreme cluster calculations (red lines), independent coordinate calculations using the ZBM (green dashed lines) and  $ps$ - $d$ - $mod$  (blue dashed-dotted lines) interactions, and two-step sequential DWBA calculations using the ZBM (orange dashed-double-dotted lines) and  $ps$ - $d$ - $mod$  (magenta dotted lines) interactions. (a) Calculations performed assuming  $J^\pi = 7/2^-$  for the 6.84 MeV state and  $J^\pi = 9/2^-$  for the 7.35 MeV state. (b)  $J^\pi = 9/2^-$  for the 6.84 MeV state and  $J^\pi = 7/2^-$  for the 7.35 MeV state.

This coefficient has been proved to be suitable for describing the elastic-scattering cross section for many systems in a wide energy range [48]. To generate single-particle and cluster wave functions the Woods-Saxon potentials were used. The depths of these potentials were varied to fit the experimental binding energies of both one and two neutrons. The reduced radii and diffuseness were set equal to 1.2 and 0.6 fm, respectively, for  $^{16}\text{O}$  and  $^{13}\text{C}$  cores. For the  $^{17}\text{O}$  and  $^{14}\text{C}$  cores, the same geometric parameters were used. The deformation parameters for the collective excitations in the entrance partition were taken from Ref. [49].

Two different models were adopted for the two-neutron transfer: The first is a direct simultaneous transfer of the two particles, and the second is a two-step sequential mechanism, which goes through the  $^{17}\text{O} + ^{14}\text{C}$  intermediate partition. The two-particle wave functions for the one-step two-neutron transfer mechanism were obtained considering three different schemes: (i) the extreme cluster model, (ii) the independent coordinate scheme, and (iii) the *microscopic cluster model*, which will be introduced in Sec. IV. Two-step DWBA calculations were performed for the sequential transfer.

The spectroscopic amplitudes were determined performing shell-model calculations with the NUSHELLX code [50] with  $^{12}\text{C}$  treated as closed core and valence protons and neutrons in the  $1p_{1/2}$ ,  $1d_{5/2}$ , and  $2s_{1/2}$  orbits. Within this model space, both positive- and negative-parity states are obtained, and in practice no spurious states exist. The effective phenomenological Zuker-Buck-McGrory (ZBM) [51] and Zuker [52] interactions were used, which allow for describing the experimental energy

spectra of both  $^{14}\text{C}$  and  $^{15}\text{C}$  nuclei with reasonable good accuracy as shown in Ref. [25]. In order to investigate the effect of the inclusion of higher-energy orbitals, a larger model space also was considered. It assumes  $^4\text{He}$  as a closed core and valence protons and neutrons in the  $1p_{3/2}$ ,  $1p_{1/2}$ ,  $1d_{5/2}$ ,  $1d_{3/2}$ , and  $2s_{1/2}$  orbits. In this case, the  $p$ - $sd$ - $mod$  interaction [53] was used. This is a modified version of the PSDWBT interaction [53] introduced by Warburton and Brown starting from the  $p$ - $sd$  part of the PSDT interaction [54]. The excitation energies obtained using the ZBM and  $p$ - $sd$ - $mod$  interactions are compared to the experimental values in Table I. For the doublets at 6.84 and 7.35 MeV, both  $7/2^-$  and  $9/2^-$  spins were considered since the spin assignment is not clear in literature [38,40]. Actually, no clear advantages result from the use of the  $p$ - $sd$ - $mod$  interaction. We even note that for most states the  $p$ - $sd$ - $mod$  interaction gives worse results than the ZBM one. The resulting two-neutron and one-neutron spectroscopic amplitudes for the ZBM interaction are listed in Tables II and III, respectively. The spectroscopic amplitudes obtained using the  $p$ - $sd$ - $mod$  interaction are not reported here for the sake of space. However, the cross sections obtained using both interactions are compared in the following.

In the extreme cluster model approximation, the relative motion between the two transferred neutrons is frozen and separated from the core. In principle, the two neutrons can couple parallel or antiparallel to an intrinsic angular momentum  $S = 0$  or  $S = 1$ , respectively. However, in the extreme cluster model calculations, we consider only the  $S = 0$  antiparallel

TABLE I. Comparison of experimental and NUSHELLX results for the  $^{13,14,15}\text{C}$  and  $^{16,17,18}\text{O}$  spectra using the ZBM and  $ps$ - $d$ -mod interactions. The spin and parity of states are shown in parentheses.

Nucleus	Experimental data		NUSHELLX data	
	$J^\pi$	Energies (MeV)	ZBM interaction Energies (MeV)	$ps$ - $d$ -mod interaction Energies (MeV)
$^{15}\text{C}$	$1/2^+$	0.0	0.0	0.0
	$5/2^+$	0.74	0.326	0.548
	$1/2^-$	3.103	2.404	1.812
	$5/2^-$	4.220	3.004	3.067
	$3/2^-$	4.657	3.639	3.828
	$7/2^-$	6.84	5.956	4.643
	$9/2^-$	7.35	5.066	4.599
	$7/2^-$	7.35	6.757	6.157
	$9/2^-$	7.35	6.757	7.744
$^{14}\text{C}$	$0^+$	0.0	0.0	0.0
	$1^-$	6.093	5.476	5.000
	$0^+$	6.589	5.781	4.777
	$3^-$	6.728	6.013	5.313
	$0^-$	6.902	6.902	6.490
	$2^+$	7.012	6.309	6.033
	$2^-$	7.341	7.140	6.377
$^{13}\text{C}$	$1/2^-$	0.0	0.0	0.0
	$1/2^+$	3.089	2.560	1.836
	$3/2^-$	3.685		3.511
	$5/2^+$	3.853	3.610	2.424
$^{16}\text{O}$	$0^+$	0.0	0.0	0.0
	$0^+$	6.049	6.353	6.983
	$3^-$	6.129	6.719	5.959
	$2^-$	8.871	9.435	8.777
$^{17}\text{O}$	$5/2^+$	0.0	0.0	0.0
	$1/2^+$	0.870	0.957	0.871
	$1/2^-$	3.055	3.254	3.536
	$5/2^-$	3.842	3.900	4.146
$^{18}\text{O}$	$0^+$	0.0	0.0	0.0
	$2^+$	1.982	2.044	2.264
	$4^+$	3.554	3.711	3.620
	$0^+$	3.633	3.746	4.251
	$3^-$	5.097	5.174	4.933

configuration. The parameters relevant for the definition of the cluster wave function are the principal quantum number  $N$  and the orbital angular momentum  $L$  relative to the core. These parameters are obtained from the conservation of the total number of quanta in the transformation of the wave function of two independent neutrons in orbits  $(n_i, l_i)$  ( $i = 1, 2$ ) into a cluster with internal state  $(n, l)$  [55]:  $2(n_1 - 1) + l_1 + 2(n_2 - 1) + l_2 = 2(N - 1) + L + 2(n - 1) + l$ . In the extreme cluster model hypothesis, we consider  $n = 1$  and  $l = 0$  so that the cluster is in a  $1s$  internal state. The spectroscopic amplitudes for both target and projectile were set to 1.0.

In the independent coordinate (IC) model, the two-neutron spectroscopic amplitudes listed in Table II were used for the ZBM case. The level scheme of the involved nuclei and the couplings adopted in the calculations are sketched in Fig. 5(a).

Two-step DWBA calculations for the sequential mechanism of two-neutron transfer also were performed in order to check the importance of the two-step mechanism. In this case, the one-neutron amplitudes in Table III were used for the ZBM case. The coupling scheme adopted in these calculations is sketched in Figs. 5(b) and 5(c) for the ZBM and  $p$ - $sd$ -mod cases, respectively.

The resulting differential cross sections for the direct (extreme cluster model and IC) and the sequential transfer are shown in Figs. 2–4. It is worth noticing that the narrow states at  $E_x = 3.103, 4.22, 4.66, 6.84,$  and  $7.35$  MeV are unbound with respect to  $S_n$ . In principle, the description of the transfer to unbound states is more involved due to the slow convergence of the open-state wave functions. Historically, such numerical difficulties have been faced using different techniques, such as

TABLE II. Spectroscopic amplitudes used in the CRC calculations with the ZBM interaction.  $j_1 j_2$  are the spins of the neutron orbitals for two-neutron transfer,  $J_{12}$  is the angular momentum of the two-neutron cluster,  $n, l, N$ , and  $L$  are the quantum numbers of the cluster wave function,  $\Lambda$  is the total orbital angular momentum, and  $S$  is the total spin of the two neutrons.

Two-neutron amplitudes—ZBM interaction											
Initial state	$j_1 j_2$	$J_{12}$	Final state	Spectroscopic amplitudes	$n$	$l$	$N$	$L$	$\Lambda$	$S$	Spectroscopic amplitudes (c.m.)
$^{18}\text{O}_{\text{g.s.}}(0^+)$	$(p_{1/2})^2$	0	$^{16}\text{O}_{\text{g.s.}}(0^+)$	0.241	1	0	2	0	0	0	0.098
	$(d_{5/2})^2$			−0.871	1	1	1	1	1	1	0.197
	$(s_{1/2})^2$			−0.367	1	0	3	0	0	0	−0.443
	$(d_{5/2})^2$			−0.871	1	1	2	1	1	1	0.389
$^{18}\text{O}_{1.98}(2^+)$	$(d_{5/2})^2$	2	$^{16}\text{O}_{\text{g.s.}}(0^+)$	0.641	1	0	2	2	2	0	0.317
	$(d_{5/2}s_{1/2})$			0.638	1	1	1	3	2	0	−0.207
	$(d_{5/2})^2$			0.641							
	$(d_{5/2}s_{1/2})$			0.638	1	1	2	1	2	0	0.1353
	$(d_{5/2})^2$			0.641	1	0	2	2	2	1	0.154
	$(d_{5/2}s_{1/2})$			0.638							
	$(d_{5/2})^2$			0.641	1	1	1	3	2	1	−0.169
	$(d_{5/2}s_{1/2})$			0.638							
	$(d_{5/2})^2$			0.641	1	1	2	1	2	1	0.110
	$(d_{5/2}s_{1/2})$			0.638							
$(d_{5/2})^2$	0.641	1	1	2	1	1	1	0.303			
$(d_{5/2})^2$	0.641	1	1	1	3	3	1	−0.122			
$^{18}\text{O}_{\text{g.s.}}(0^+)$	$(p_{1/2}d_{5/2})$	3	$^{16}\text{O}_{6.13}(3^-)$	0.801	1	0	1	3	3	0	−0.283
				0.801	1	1	1	2	3	0	0.163
				0.801	1	0	1	3	3	1	0.327
				0.801	1	1	1	2	2	1	0.267
$^{13}\text{C}_{\text{g.s.}}(1/2^-)$	$(p_{1/2}s_{1/2})$	0	$^{15}\text{C}_{\text{g.s.}}(1/2^+)$	−0.641	1	0	2	1	1	1	−0.292
				−0.641	1	1	1	2	1	1	0.338
				−0.641	1	1	2	0	1	1	−0.075
		−1.110		1	0	2	1	1	0	0.292	
		−1.110		1	1	1	2	1	0	−0.338	
		−1.110		1	1	2	0	1	0	0.075	
$^{13}\text{C}_{\text{g.s.}}(1/2^-)$	$(p_{1/2}s_{1/2})$	1	$^{15}\text{C}_{0.74}(5/2^+)$	−1.110	1	0	2	1	1	1	−0.413
				−1.110	1	1	1	2	1	1	0.477
		−0.231		1	1	2	0	1	1	−0.107	
		−0.231		1	0	2	1	1	1	−0.231	
		0.210		1	1	1	2	2	0	0.210	
		−0.133		1	1	1	2	1	1	−0.133	
		0.298		1	1	2	0	1	1	0.298	
		−0.344		1	1	1	2	2	1	−0.344	
		−0.088		1	0	1	3	3	1	−0.088	
		0.051		1	1	1	2	3	1	0.051	
$^{13}\text{C}_{\text{g.s.}}(1/2^-)$	$(p_{1/2}d_{5/2})$	2	$^{15}\text{C}_{3.103}(1/2^-)$	−0.815	1	0	1	3	3	1	−0.394
				−0.815	1	0	1	3	3	0	0.341
		−0.964		1	1	1	2	3	0	−0.197	
		−0.964		1	1	1	2	2	1	−0.321	
		−0.964		1	1	1	2	3	1	0.227	
		−0.964		1	1	1	2	3	1	0.227	
$^{13}\text{C}_{\text{g.s.}}(1/2^-)$	$(d_{5/2})^2$	0	$^{15}\text{C}_{3.103}(1/2^-)$	0.573	1	0	3	0	0	0	0.555
	$(s_{1/2})^2$			0.820	1	1	2	1	0	0	0
	$(d_{5/2})^2$			0.573							
	$(s_{1/2})^2$			0.820	1	1	2	1	1	1	−0.256
	$(d_{5/2})^2$			0.820	1	1	2	1	1	1	−0.256
	$(p_{1/2})^2$			0	1	0	2	0	0	0	0
$(p_{1/2})^2$	0	1	1	1	0	0	0	0			
$(p_{1/2})^2$	0	1	1	1	1	1	1	0			

TABLE II. (Continued.)

Two-neutron amplitudes—ZBM interaction											
Initial state	$j_1 j_2$	$J_{12}$	Final state	Spectroscopic amplitudes	$n$	$l$	$N$	$L$	$\Lambda$	$S$	Spectroscopic amplitudes (c.m.)
$^{13}\text{C}_{\text{g.s.}}(1/2^-)$	$(d_{5/2})^2$	2	$^{15}\text{C}_{4.22}(5/2^-)$	0.477	1	0	2	2	2	0	0.354
	$(d_{5/2}s_{1/2})$			0.874	1	1	1	3	2	0	-0.283
	$(d_{5/2})^2$			0.477	1	1	2	1	2	0	0.185
	$(d_{5/2}s_{1/2})$			0.874	1	0	2	2	2	1	0.211
	$(d_{5/2})^2$			0.477	1	1	1	3	2	1	-0.231
	$(d_{5/2}s_{1/2})$			0.874	1	1	2	1	2	1	0.151
	$(d_{5/2})^2$			0.477	1	1	2	1	1	1	0.226
	$(d_{5/2}s_{1/2})$			0.874	1	1	1	3	3	1	-0.090
	$(d_{5/2})^2$			0.477	1	0	2	2	2	1	0.035
	$(d_{5/2}s_{1/2})$			0.093	1	1	1	3	2	1	-0.039
					1	1	2	1	2	1	0.025
$^{13}\text{C}_{\text{g.s.}}(1/2^-)$	$(d_{5/2})^2$	2	$^{15}\text{C}_{4.66}(3/2^-)$	0.426	1	0	2	2	2	0	0.353
	$(d_{5/2}s_{1/2})$			0.905	1	1	1	3	2	0	-0.293
	$(d_{5/2})^2$			0.426	1	1	2	1	2	0	0.192
	$(d_{5/2}s_{1/2})$			0.905	1	0	2	2	2	1	0.219
	$(d_{5/2})^2$			0.426	1	1	1	3	2	1	-0.239
	$(d_{5/2}s_{1/2})$			0.905	1	1	2	1	2	1	0.157
	$(d_{5/2})^2$			0.426	1	1	2	1	1	1	0.201
	$(d_{5/2}s_{1/2})$			0.905	1	1	1	3	3	1	-0.081
	$(d_{5/2})^2$			0.426	1	0	1	4	4	0	0.274
	$(d_{5/2})^2$			1.0	1	1	1	3	3	1	0.632
$^{13}\text{C}_{\text{g.s.}}(1/2^-)$	$(d_{5/2})^2$	4	$^{15}\text{C}_{6.84}(9/2^-)$	1.0	1	0	1	4	4	1	0
				1	1	1	3	4	0	0	
				1	1	1	3	4	0	0	
				1	1	1	3	4	1	0	
$^{13}\text{C}_{\text{g.s.}}(1/2^-)$	$(d_{5/2}s_{1/2})$	3	$^{15}\text{C}_{7.35}(7/2^-)$	0.0	1	0	2	2	2	1	0
				1	1	1	3	2	1	0	
				1	1	2	1	2	1	0	
$^{13}\text{C}_{\text{g.s.}}(1/2^-)$	$(d_{5/2})^2$	4	$^{15}\text{C}_{7.35}(7/2^-)$	1.0	1	0	1	4	4	0	0.274
				1	1	1	3	3	1	0.632	
				1	0	1	4	4	1	0	
				1	1	1	3	4	0	0	
				1	1	1	3	4	1	0	

(i) the bound state approximation [56] in which the scattering state is replaced by a weakly bound wave function with the same quantum numbers; (ii) the use of a convergence factor in the scattering state [57]; (iii) the technique by Vincent and Fortune [58], which adopts the actual scattering state choosing an appropriate integration contour along the complex

plane, thus improving the convergence. Another approach is the continuum discretized coupled channels [59] in which the continuum states are discretized in energy bins on the order of the energy resolution of the experiment. Such methods were extensively used in the description of single-particle states populated by  $(d, p)$  or  $(d, n)$  reactions. In our case,

TABLE III. Spectroscopic amplitudes used in the DWBA calculations with the ZBM interaction.  $J$  is the spin of the neutron orbital for the one-neutron transfer.

One-neutron amplitudes—ZBM interaction			
Initial state	$J$	Final state	Spectroscopic amplitude
$^{18}\text{O}_{\text{g.s.}}(0^+)$	$d_{5/2}$	$^{17}\text{O}_{\text{g.s.}}(5/2^+)$	1.304
	$s_{1/2}$	$^{17}\text{O}_{0.870}(1/2^+)$	-0.561
	$p_{1/2}$	$^{17}\text{O}_{3.055}(1/2^-)$	-0.929
$^{18}\text{O}_{1.98}(2^+)$	$s_{1/2}$	$^{17}\text{O}_{\text{g.s.}}(5/2^+)$	0.666
	$d_{5/2}$	$^{17}\text{O}_{0.870}(1/2^+)$	0.929
	$d_{5/2}$	$^{17}\text{O}_{0.870}(1/2^+)$	-0.652
	$p_{1/2}$	$^{17}\text{O}_{3.842}(5/2^-)$	0.825
$^{17}\text{O}_{\text{g.s.}}(5/2^+)$	$d_{5/2}$	$^{16}\text{O}_{\text{g.s.}}(0^+)$	-0.973
	$p_{1/2}$	$^{16}\text{O}_{6.129}(3^-)$	-0.718
$^{17}\text{O}_{0.870}(1/2^+)$	$s_{1/2}$	$^{16}\text{O}_{\text{g.s.}}(0^+)$	0.975
$^{17}\text{O}_{3.055}(1/2^-)$	$p_{1/2}$	$^{16}\text{O}_{\text{g.s.}}(0^+)$	-0.291
	$d_{5/2}$	$^{16}\text{O}_{6.129}(3^-)$	-0.609
$^{17}\text{O}_{3.842}(5/2^-)$	$s_{1/2}$	$^{16}\text{O}_{6.129}(3^-)$	-0.588
	$d_{5/2}$	$^{16}\text{O}_{6.129}(3^-)$	-0.718
$^{13}\text{C}_{\text{g.s.}}(1/2^-)$	$p_{1/2}$	$^{14}\text{C}_{\text{g.s.}}(0^+)$	1.291
	$s_{1/2}$	$^{14}\text{C}_{6.093}(1^-)$	-1.0
	$p_{1/2}$	$^{14}\text{C}_{6.589}(0^+)$	-0.412
	$d_{5/2}$	$^{14}\text{C}_{6.728}(3^-)$	-1.0
	$s_{1/2}$	$^{14}\text{C}_{6.902}(0^-)$	1.0
	$d_{5/2}$	$^{14}\text{C}_{7.341}(2^-)$	1.0
$^{14}\text{C}_{\text{g.s.}}(0^+)$	$s_{1/2}$	$^{15}\text{C}_{\text{g.s.}}(1/2^+)$	0.975
	$d_{5/2}$	$^{15}\text{C}_{0.74}(5/2^+)$	0.975
$^{14}\text{C}_{6.093}(1^-)$	$p_{1/2}$	$^{15}\text{C}_{\text{g.s.}}(1/2^+)$	1.110
	$s_{1/2}$	$^{15}\text{C}_{3.103}(1/2^-)$	-1.004
	$d_{5/2}$	$^{15}\text{C}_{4.22}(5/2^-)$	-0.727
	$d_{5/2}$	$^{15}\text{C}_{4.66}(3/2^-)$	-0.905
$^{14}\text{C}_{6.589}(0^+)$	$s_{1/2}$	$^{15}\text{C}_{\text{g.s.}}(1/2^+)$	-0.179
	$d_{5/2}$	$^{15}\text{C}_{0.74}(5/2^+)$	0.032
	$p_{1/2}$	$^{15}\text{C}_{3.103}(1/2^-)$	-0.882
$^{14}\text{C}_{6.728}(3^-)$	$p_{1/2}$	$^{15}\text{C}_{0.74}(5/2^+)$	0.964
	$d_{5/2}$	$^{15}\text{C}_{3.103}(1/2^-)$	-0.619
	$s_{1/2}$	$^{15}\text{C}_{4.22}(5/2^-)$	-0.846
	$d_{5/2}$	$^{15}\text{C}_{4.66}(3/2^-)$	-0.584
	$d_{5/2}$	$^{15}\text{C}_{4.66}(3/2^-)$	-0.347
	$d_{5/2}$	$^{15}\text{C}_{6.84}(9/2^-)$	-1.354
	$s_{1/2}$	$^{15}\text{C}_{7.35}(7/2^-)$	0.0
$d_{5/2}$	$^{15}\text{C}_{7.35}(7/2^-)$	-0.577	
$^{14}\text{C}_{6.902}(0^-)$	$p_{1/2}$	$^{15}\text{C}_{\text{g.s.}}(1/2^+)$	-0.641
	$s_{1/2}$	$^{15}\text{C}_{3.103}(1/2^-)$	-0.580
	$d_{5/2}$	$^{15}\text{C}_{4.22}(5/2^-)$	-0.493
$^{14}\text{C}_{7.012}(2^+)$	$d_{5/2}$	$^{15}\text{C}_{\text{g.s.}}(1/2^+)$	0.353
	$s_{1/2}$	$^{15}\text{C}_{0.74}(5/2^+)$	0.204
	$d_{5/2}$	$^{15}\text{C}_{0.74}(5/2^+)$	0.142
	$p_{1/2}$	$^{15}\text{C}_{4.22}(5/2^-)$	0.993
	$p_{1/2}$	$^{15}\text{C}_{4.66}(3/2^-)$	1.0
$^{14}\text{C}_{7.341}(2^-)$	$p_{1/2}$	$^{15}\text{C}_{0.74}(5/2^+)$	-0.815
	$d_{5/2}$	$^{15}\text{C}_{3.103}(1/2^-)$	-0.527
	$s_{1/2}$	$^{15}\text{C}_{4.22}(5/2^-)$	-0.237
	$d_{5/2}$	$^{15}\text{C}_{4.22}(5/2^-)$	-0.337
	$d_{5/2}$	$^{15}\text{C}_{6.84}(9/2^-)$	-0.408
$d_{5/2}$	$^{15}\text{C}_{7.35}(7/2^-)$	1.291	

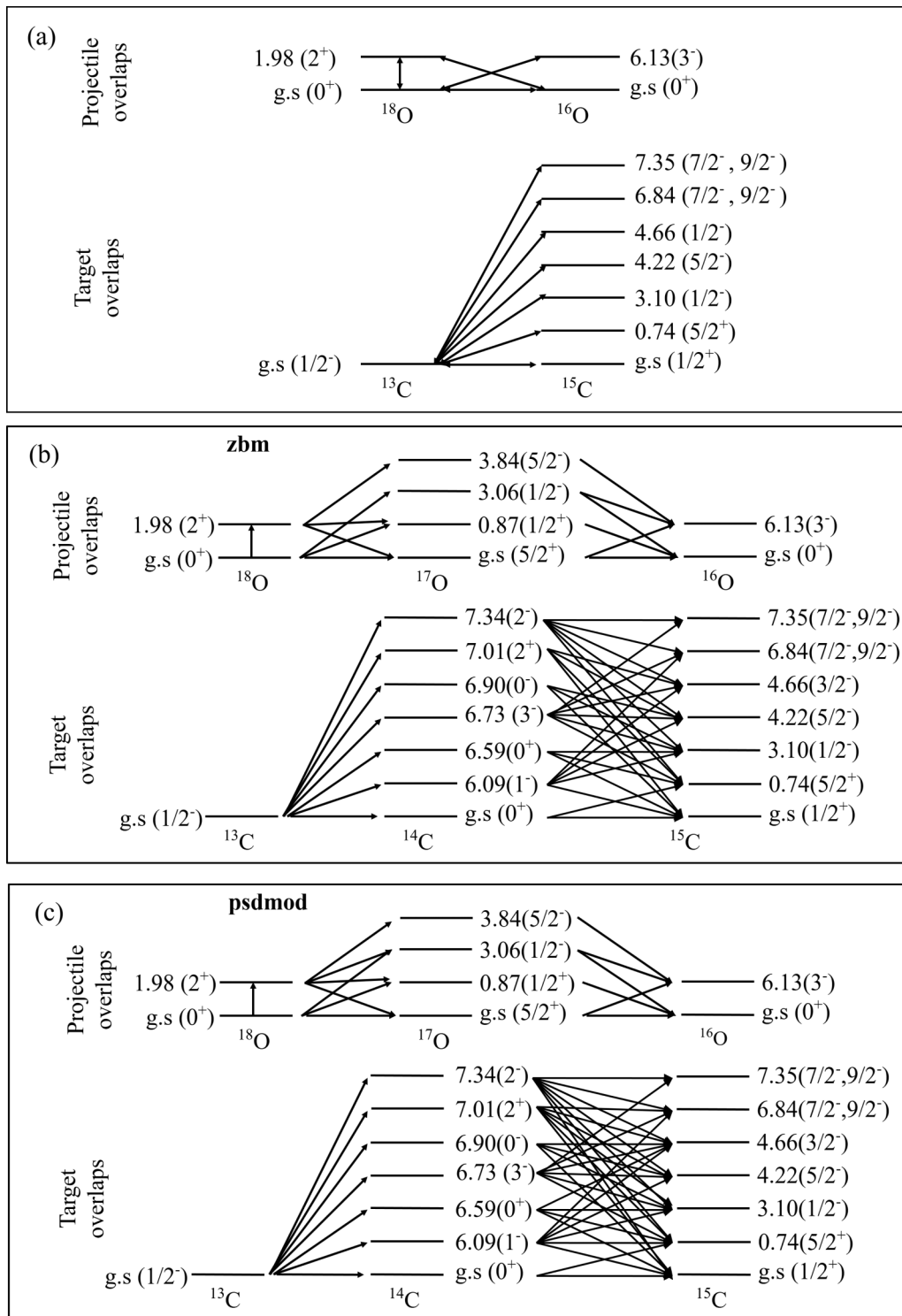


FIG. 5. Coupling scheme for (a) direct two-neutron transfer and (b) and (c) sequential two-neutron transfer with the ZBM and *ps-d*-mod interactions, respectively.

the above-mentioned resonances are bound compared to the two-neutron emission ( $S_{2n} = 9.39$  MeV), and the dominant component for these states consists of a *p*-shell neutron hole coupled with a two-neutron pair in the *sd* shell [38]. Consequently, they can be treated safely as quasibound states in our structure model for the two-nucleon transfer CRC

calculations. In particular, the results for transfer to the ground state and the states at 0.74 and 3.103 MeV of  $^{15}\text{C}$  are presented in Fig. 2. For these transitions, the extreme cluster model calculations give much larger cross sections than the data, the only exception being the transition to the first excited state at 0.74 MeV for which this model provides the best description.

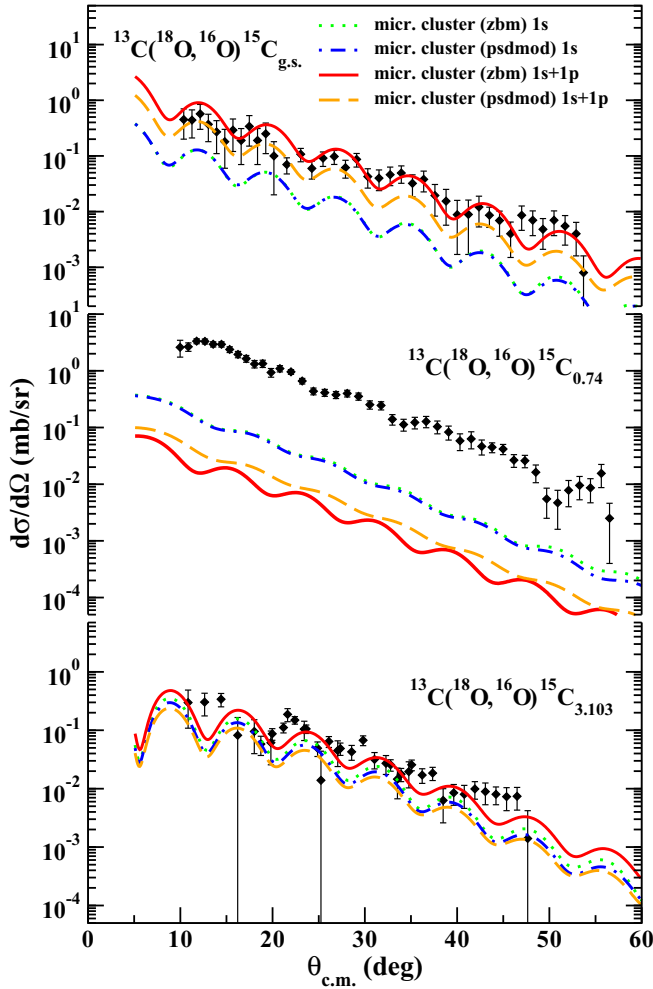


FIG. 6. Experimental cross-section angular distributions for the transitions to the ground state and states at 0.74 and 3.103 MeV in  $^{15}\text{C}$ . Theoretical calculations (see the text):  $1s$  microscopic cluster calculations using the ZBM (green dotted lines) and  $ps$ - $d$ -mod (blue dashed-dotted lines) interactions and  $1s + 1p$  microscopic cluster calculations using the ZBM (red lines) and  $ps$ - $d$ -mod (orange dashed lines) interactions.

The IC calculations describe quite well the cross section for the ground state and the state at 3.103 MeV. Moreover, the results obtained using the two interactions ZBM and  $p$ - $sd$  mod are similar in the IC calculations, whereas the two-step sequential DWBA calculations with the  $p$ - $sd$ -mod interaction are lower than the calculations using the ZBM interaction.

For the transitions to the resonances at 4.22 and 4.66 MeV, the two-step DWBA calculations with both  $p$ - $sd$ -mod and ZBM interactions (see Fig. 3) underestimate the experimental cross section, but the factor is significantly smaller for the ZBM interaction. The IC calculations with the ZBM interaction describe quite well the experimental data for both transitions, and when using the  $p$ - $sd$ -mod interaction only slightly lower cross sections are obtained.

As already mentioned, the states of the doublet at 6.84 and 7.35 MeV have no firm spin assignment, thus both the expected spin-parity values ( $9/2^-$ ,  $7/2^-$ ) were computed

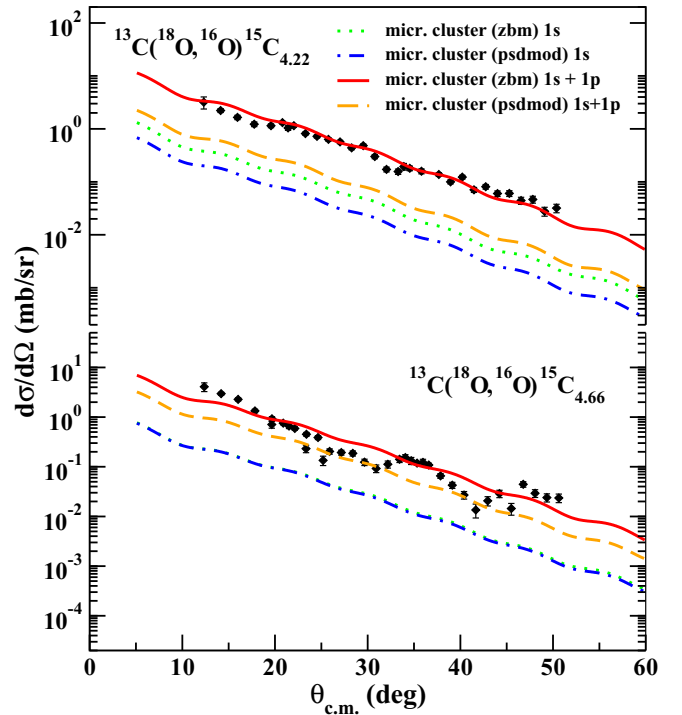


FIG. 7. Experimental cross-section angular distributions for the transitions to the 4.22 and 4.66 MeV states in  $^{15}\text{C}$ . Theoretical calculations (see the text):  $1s$  microscopic cluster calculations using the ZBM (green dotted lines) and  $ps$ - $d$ -mod (blue dashed-dotted lines) interactions and  $1s + 1p$  microscopic cluster calculations using the ZBM (red lines) and  $ps$ - $d$ -mod (orange dashed lines) interactions.

for each transition (see Table I). The results are shown in Fig. 4. The extreme cluster calculations describe quite well the experimental cross sections for these transitions. Regarding the IC calculations using the ZBM interaction, the only possible assignment is  $9/2^-$  for the 6.84 MeV state and  $7/2^-$  for the 7.35 MeV state since in the corresponding model space there is only one  $9/2^-$  state and it is below the  $7/2^-$  state. The obtained results are a bit lower than the data in this case [see Fig. 4(b)]. With the  $p$ - $sd$ -mod interaction, both possibilities were calculated, but the results for the transition at 6.84 MeV ( $7/2^-$ ) poorly reproduce the data [see Fig. 4(a)] with both interactions. The two-step DWBA calculations give cross-sections orders of magnitude lower than the data.

The present IC calculations would suggest  $J^\pi = 9/2^-$  for the state at 6.84 MeV, which is in agreement with the spin assignment discussed in Ref. [40]. For the state at 7.35 MeV, the situation is less clear since a reasonable agreement between theoretical and experimental angular distributions is obtained for  $J^\pi = 7/2^-$  using the ZBM interaction and for  $J^\pi = 9/2^-$  using the  $p$ - $sd$ -mod one.

To summarize, the theoretical cross sections reproduce reasonably well the experimental data for CRC calculations. Two-step sequential DWBA calculations are in some cases on the same order of magnitude but always lower than the data. The theoretical cross sections corresponding to the direct (correlated) two-neutron transfer describe quite well the experimental angular distributions in the case of the

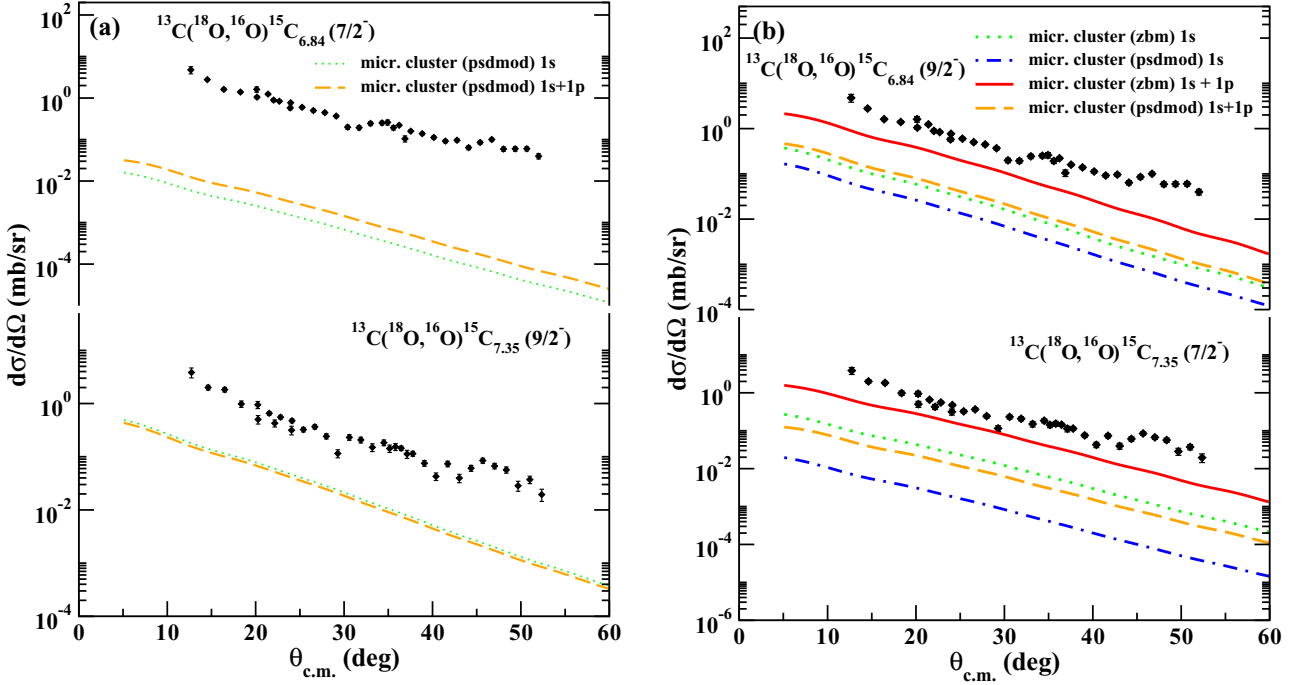


FIG. 8. Experimental cross-section angular distributions for the transitions to the 6.84 and 7.35 MeV states in  $^{15}\text{C}$ . Theoretical calculations (see the text):  $1s$  microscopic cluster calculations using the ZBM (green dotted lines) and  $ps$ - $d$ -mod (blue dashed-dotted lines) interactions and  $1s + 1p$  microscopic cluster calculations using the ZBM (red lines) and  $ps$ - $d$ -mod (orange dashed lines) interactions. Left panel: calculations performed assuming  $J^\pi = 7/2^-$  for the 6.84 MeV state and  $J^\pi = 9/2^-$  for the 7.35 MeV state. Right panel:  $J^\pi = 9/2^-$  for the 6.84 MeV state and  $J^\pi = 7/2^-$  for the 7.35 MeV state.

independent coordinate model. These results are in agreement with those recently obtained for the  $^{12}\text{C}(^{18}\text{O}, ^{16}\text{O})^{14}\text{C}$  reaction at the same energy [25]. The two-neutron correlation discussed in Ref. [25] is present also in this case, even with the presence of the extra neutron in  $^{13}\text{C}$ , which seems to not influence the reaction dynamics. Regarding the two bound states (g.s. and 0.74 MeV), as already mentioned, these are referred to in literature as single-particle states [39], and indeed in the present reaction they show lower cross sections with respect to the strong populated two-particle states (i.e., states at 4.22, 4.66, 6.84, and 7.35 MeV). The low cross sections that we observe for these two transitions are due to the hindered excitation of  $^{14}\text{C}_{\text{g.s.}}$  components, such as  $|^{12}\text{C}_{\text{g.s.}}(0^+) \otimes (2s_{1/2})_{2\nu}\rangle$  or  $|^{12}\text{C}_{\text{g.s.}}(0^+) \otimes (1d_{5/2})_{2\nu}\rangle$  since we are starting from  $|^{13}\text{C}_{\text{g.s.}}(1/2^-)\rangle = |^{12}\text{C}_{\text{g.s.}}(0^+) \otimes (1p_{1/2})_{\nu}\rangle$ . The single-particle nature of the ground and first excited states is confirmed by the calculations. Indeed, the sequential DWBA calculations give a strong contribution for the transitions to these two states (see Fig. 2), whereas this is not the case for the transitions to the strongly populated two-particle states (see Figs. 3 and 4).

### A. The microscopic cluster model

In the case of the extreme cluster model with spectroscopic amplitudes set to 1.0, the calculated cross sections are larger than the experimental data. The main reason for this overestimation might lie in the approximation that the two neutrons are coupled to the total spin  $S = 0$  with 100% probability. A natural way to go beyond this ansatz is to

introduce both parallel and antiparallel couplings for the two neutrons. Realistic spectroscopic amplitudes are required for all the possible combinations of single-particle configurations in this enlarged space. These can be derived from shell-model calculations, and we refer to this approach as the microscopic cluster model. To achieve this goal, we made use of transformations from individual ( $j$ - $j$  coupling) to relative and center-of-mass coordinates ( $LS$  coupling) for the harmonic-oscillator wave functions of the two-particle system. Thus, the cluster spectroscopic factors can be written as

$$\begin{aligned}
 S_{\alpha J \beta J'}[(nl)(NL)\Lambda S; J] \\
 = \sum_{n_1 l_1 n_2 l_2} \sum_{j_1 j_2} \hat{S} \hat{L} \hat{j}_1 \hat{j}_2 \begin{Bmatrix} l_1 & 1/2 & j_1 \\ l_2 & 1/2 & j_2 \\ \Lambda & S & J \end{Bmatrix} C^L(n_1 l_1 n_2 l_2; n l N L) \\
 \times S_{\alpha J \beta J'}[n_1 l_1 j_1 n_2 l_2 j_2; J], \quad (1)
 \end{aligned}$$

where  $\hat{a} = \sqrt{2a + 1}$  with  $a = S, L, j_1$ , and  $j_2$ ; the expressions in the braces are  $9j$  coefficients;  $C^L(n_1 l_1 n_2 l_2; n l N L)$  stands for the Moshinsky brackets [55]; and  $S_{\alpha J \beta J'}[n_1 l_1 j_1 n_2 l_2 j_2; J]$  are the two-neutron spectroscopic factors in the  $j$ - $j$  coupling in Table II. The spectroscopic amplitudes obtained using this transformation are given in Table II for the ZBM interaction. In what follows, we call this approach the *microscopic cluster calculations*.

As a first step, we performed microscopic cluster calculations considering that the cluster relative motion state is represented exclusively by  $n = 1$  and  $l = 0$  quantum numbers, i.e., the cluster is in the  $1s$  intrinsic state. The results of

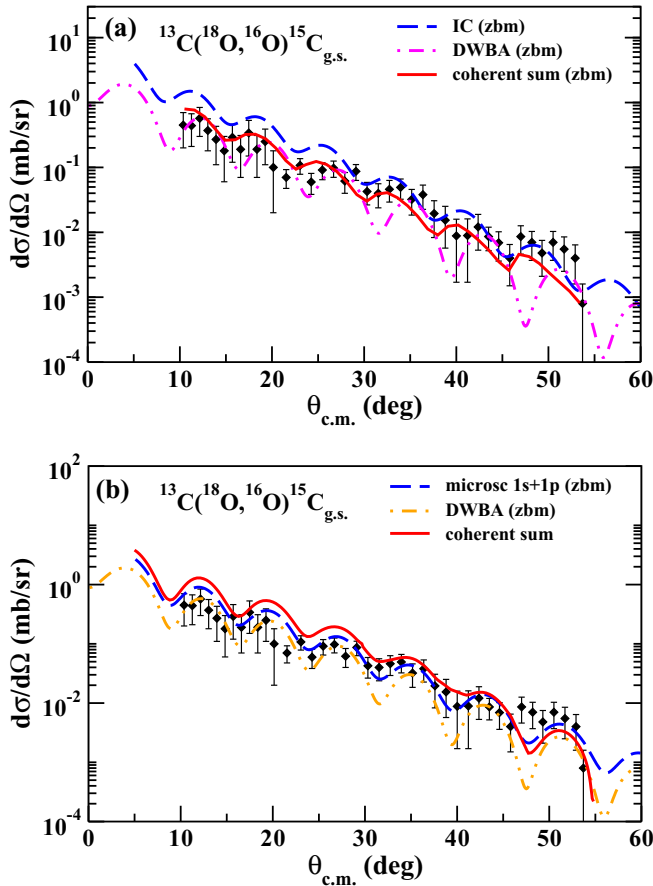


FIG. 9. Experimental cross-section angular distributions for the transitions to the ground state in  $^{15}\text{C}$ . Theoretical calculations (see the text): (a) coherent sum (red line) of the sequential DWBA calculations (pink dotted-dashed line) and the IC calculation (blue dashed line) using the ZBM interaction; (b) coherent sum (red line) of the DWBA calculation (orange dashed-dotted line) and the  $1s + 1p$  microscopic cluster calculation (blue dashed line) using the ZBM interaction.

these calculations are shown in Figs. 6–8. The obtained cross sections (labeled as the  $1s$  microscopic cluster) are much lower than data for all transitions. Thus, we also included the  $1p$  ( $n = 1$  and  $l = 1$ ) cluster relative motion states, and the results are shown in Figs. 6–8 (labeled as the  $1s + 1p$  microscopic cluster). In particular, the results for transfer to the ground state and the states at 0.74 and 3.103 MeV of  $^{15}\text{C}$  are displayed in Fig. 6. We see that the results of the  $1s + 1p$  microscopic cluster calculations are in rather good agreement with the experimental angular distributions for the ground state and the state at 3.103 MeV. However, in the case of the 0.74 MeV state, the addition of the  $1p$  wave decreases the cross section. This is probably due to a destructive interference between the  $1s$  and the  $1p$  waves. Regarding the used interactions, the ZBM interaction gives better results than the  $ps$ - $d$ -mod interaction. This behavior also is observed for the transition to the resonances at 4.22 and 4.66 MeV, shown in Fig. 7. The  $1s + 1p$  microscopic cluster calculations with the ZBM interaction describe very well the experimental data for both transitions. Finally, for

the doublet ( $9/2^-$ ,  $7/2^-$ ) at 6.84 and 7.35 MeV, the results are shown in Fig. 8. In this case, the microscopic cluster calculations underestimate the experimental cross section, but the best result is obtained again with the  $1s + 1p$  waves and the ZBM interaction. Again, the best description of this doublet is obtained by considering the  $J^\pi = 9/2^-$  for the 6.84 MeV state and  $J^\pi = 7/2^-$  for the 7.35 MeV state.

The microscopic cluster model also was applied to describe the  $^{12}\text{C}(^{18}\text{O}, ^{16}\text{O})^{14}\text{C}$  transitions at 84 MeV incident energy, already analyzed in Ref. [25]. The results also are quite good in this case. In particular, for  $^{14}\text{C}_{\text{g.s.}}$  the  $1s$  microscopic cluster calculation is found to be the dominant component; indeed by adding the  $1p$  wave to the microscopic calculation for  $^{14}\text{C}_{\text{g.s.}}$ , a maximum increasing of 20% in the cross section is observed. This was expected since this state is known to be characterized by a strong cluster configuration [25].

As already mentioned, a complete treatment of the transfer process is still not available in the state-of-the-art theories. For this reason, in our theoretical analysis, we performed separate calculations for the direct and the sequential reaction mechanisms. As described in Refs. [25,26], it is possible to perform the coherent sum of these two components with an arbitrary phase determined from the reduced least  $\chi^2$  value obtained in the whole range of phases. In Fig. 9, we show the coherent sum of the sequential DWBA cross sections and the independent coordinate calculations ( $\chi^2 = 1.08$  with the phase  $139.8^\circ$ ) [Fig. 9(a)] and the  $1s + 1p$  microscopic cluster ( $\chi^2 = 1.17$  with the phase  $97.4^\circ$ ) [Fig. 9(b)] for the transition to the ground state using in both cases the ZBM interaction. The interference between the direct and the sequential mechanisms provides little improvement in the description of the experimental data in the case of the IC calculations.

## V. SUMMARY AND CONCLUSIONS

In the present paper we reported the cross-section angular distributions obtained for the two-neutron transfer reaction  $^{13}\text{C}(^{18}\text{O}, ^{16}\text{O})^{15}\text{C}$  at the  $^{18}\text{O}$  laboratory energy of 84 MeV. The experimental cross sections for the population of the states in  $^{15}\text{C}$  are reasonably well described by one-step CRC calculations with no need for any “unhappiness” factor. Three models were used to calculate the cross sections: the extreme cluster model, the independent coordinate model, and the microscopic cluster model.

In particular, the microscopic cluster model, developed here for the first time, has allowed for describing rather well the experimental cross sections for most of the transitions thus demonstrating the importance of a two-neutron correlation in the nuclear wave function in the two-neutron transfer mechanism. A dominance of the  $1s$  and  $1p$  waves in the two-neutron cluster internal wave function is found. This result shows that the extra neutron in  $^{13}\text{C}$  when compared to  $^{12}\text{C}$  does not destroy the neutron-neutron correlations in the wave functions.

In addition, we have found that the ZBM interaction, which includes the  $1p_{1/2}$ ,  $1d_{5/2}$ , and  $2s_{1/2}$  orbits out of a  $^{12}\text{C}$  core, allows a good description of the experimental findings. The further inclusion of the  $1p_{3/2}$  and  $1d_{3/2}$  orbits using the  $ps$ - $d$ -mod interaction do not give any improvement; indeed

it worsens the results. This is probably because most of the states under investigation, except resonances at higher excitation energy, do not significantly involve correlations outside of the  $1p_{1/2}$ ,  $1d_{5/2}$ , and  $2s_{1/2}$  model space. These correlations are well accounted for by the ZBM interaction

which is specifically developed for this mass region. However, we find that to improve the results for the resonance at higher excitation energy, e.g., 6.84 and 7.35 MeV, where the  $1d_{3/2}$  orbit starts to be important, it would be necessary to develop a new interaction.

- 
- [1] R. A. Broglia and A. Winther, *Heavy-Ion Reactions* (Addison-Wesley, Reading, MA, 1981).
- [2] S. Mordechai *et al.*, *Nucl. Phys. A* **301**, 463 (1978).
- [3] P. Guazzoni *et al.*, *Phys. Rev. C* **83**, 044614 (2011).
- [4] P. Guazzoni *et al.*, *Phys. Rev. C* **78**, 064608 (2008).
- [5] P. Guazzoni *et al.*, *Phys. Rev. C* **74**, 054605 (2006).
- [6] P. Guazzoni *et al.*, *Phys. Rev. C* **69**, 024619 (2004).
- [7] G. Potel, F. Barranco, F. Marini, A. Idini, E. Vigezzi, and R. A. Broglia, *Phys. Rev. Lett.* **107**, 092501 (2011).
- [8] G. Potel, F. Barranco, E. Vigezzi, and R. A. Broglia, *Phys. Rev. Lett.* **105**, 172502 (2010).
- [9] G. Potel *et al.*, *EPJ Web Conf.* **17**, 01004 (2011).
- [10] F. Cappuzzello, C. Agodi, D. Carbone, and M. Cavallaro, *Eur. Phys. J. A* **52**, 167 (2016).
- [11] A. Cunsolo *et al.*, *Nucl. Instrum. Methods Phys. Res., Sect. A* **481**, 48 (2002).
- [12] A. Cunsolo *et al.*, *Nucl. Instrum. Methods Phys. Res., Sect. A* **484**, 56 (2002).
- [13] D. Carbone *et al.*, *Phys. Rev. C* **90**, 064621 (2014).
- [14] M. Cavallaro *et al.*, *J. Phys.: Conf. Ser.* **381**, 012094 (2012).
- [15] D. Nicolosi *et al.*, *Acta Phys. Pol., B* **44**, 657 (2013).
- [16] D. Carbone *et al.*, *Acta Phys. Pol., B* **45**, 431 (2014).
- [17] D. Carbone *et al.*, *J. Phys.: Conf. Ser.* **590**, 012030 (2015).
- [18] D. Carbone *et al.*, *J. Phys.: Conf. Ser.* **312**, 082016 (2011).
- [19] F. Cappuzzello *et al.*, *Nat. Commun.* **6**, 6743 (2015).
- [20] D. Carbone, *Eur. Phys. J. Plus* **130**, 143 (2015).
- [21] F. Cappuzzello *et al.*, *Phys. Lett. B* **711**, 347 (2012).
- [22] M. Cavallaro *et al.*, *Phys. Rev. C* **93**, 064323 (2016).
- [23] H. Laurent *et al.*, *Nucl. Instrum. Methods Phys. Res., Sect. A* **326**, 517 (1993).
- [24] M. Cavallaro *et al.*, *Nucl. Instrum. Methods Phys. Res., Sect. A* **700**, 65 (2013).
- [25] M. Cavallaro *et al.*, *Phys. Rev. C* **88**, 054601 (2013).
- [26] M. J. Ermamatov *et al.*, *Phys. Rev. C* **94**, 024610 (2016).
- [27] M. Cavallaro *et al.*, in *Two-Neutron Stripping in ( $^{18}\text{O}$ ,  $^{16}\text{O}$ ) and ( $t,p$ ) Reactions*, edited by M. H. Tabacniks, J. R. Brandão de Oliveira, J. M. Barbosa Shorto, and R. Higa, AIP Conf. Proc. No. 1625 (AIP, New York, 2014), p. 38.
- [28] P. D. Bond, H. J. Korner, M.-C. Lemaire, D. J. Pisano, and C. E. Thorn, *Phys. Rev. C* **16**, 177 (1977).
- [29] M.-C. Lemaire and K. S. Low, *Phys. Rev. C* **16**, 183 (1977).
- [30] D. Pereira *et al.*, *Phys. Lett. B* **710**, 426 (2012).
- [31] G. R. Satchler, *Direct Nuclear Reactions* (Oxford University Press, Oxford, 1983).
- [32] I. J. Thompson, *Comput. Phys. Rep.* **7**, 167 (1988).
- [33] F. Cappuzzello *et al.*, *Nucl. Instrum. Methods Phys. Res., Sect. A* **621**, 419 (2010).
- [34] F. Cappuzzello *et al.*, *Nucl. Instrum. Methods Phys. Res., Sect. A* **638**, 74 (2011).
- [35] M. Cavallaro *et al.*, *Nucl. Instrum. Methods Phys. Res., Sect. A* **637**, 77 (2011).
- [36] M. Cavallaro *et al.*, *Eur. Phys. J. A* **48**, 59 (2012).
- [37] D. Carbone, F. Cappuzzello, and M. Cavallaro, *Eur. Phys. J. A* **48**, 60 (2012).
- [38] S. Truong and H. T. Fortune, *Phys. Rev. C* **28**, 977 (1983).
- [39] G. Murillo, S. Sen, and S. E. Darden, *Nucl. Phys. A* **579**, 125 (1994).
- [40] H. G. Bohlen *et al.*, *Phys. Rev. C* **68**, 054606 (2003).
- [41] S. E. Darden, G. Murillo, and S. Sen, *Phys. Rev. C* **32**, 1764 (1985).
- [42] J. D. Goss *et al.*, *Phys. Rev. C* **8**, 514 (1973).
- [43] F. Cappuzzello *et al.*, *Europhys. Lett.* **65**, 766 (2004).
- [44] S. E. A. Orrigo *et al.*, *Phys. Lett. B* **633**, 469 (2006).
- [45] J. I. Thompson, <http://www.fresco.org.uk/>
- [46] L. C. Chamon *et al.*, *Phys. Rev. C* **66**, 014610 (2002).
- [47] D. Pereira *et al.*, *Phys. Lett. B* **670**, 330 (2009).
- [48] L. R. Gasques *et al.*, *Nucl. Phys. A* **764**, 135 (2006).
- [49] S. Raman, C. W. Nestor, Jr., and P. Tikkanen, *At. Data Nucl. Data Tables* **78**, 1 (2001).
- [50] W. D. M. Rae, <http://www.garsington.eclipse.co.uk/>
- [51] A. P. Zuker, B. Buck, and J. B. McGrory, *Phys. Rev. Lett.* **21**, 39 (1968).
- [52] A. P. Zuker, *Phys. Rev. Lett.* **23**, 983 (1969).
- [53] Y. Utsuno and S. Chiba, *Phys. Rev. C* **83**, 021301 (2011).
- [54] E. K. Warburton and B. A. Brown, *Phys. Rev. C* **46**, 923 (1992).
- [55] M. Moshinsky, *Nucl. Phys.* **13**, 104 (1959).
- [56] W. R. Coker, *Phys. Rev. C* **9**, 784 (1974).
- [57] R. Huby and J. R. Mines, *Rev. Mod. Phys.* **37**, 406 (1965).
- [58] C. M. Vincent and H. T. Fortune, *Phys. Rev. C* **2**, 782 (1970).
- [59] N. Austern *et al.*, *Phys. Rep.* **154**, 125 (1987).